Journal of Computational Physics **182,** 622–645 (2002)
doi:10.1006/jcph.2002.7189

Simulation of Pore-Scale Dispersion in Periodic Porous Media Using Smoothed Particle Hydrodynamics

Yi Zhu* and Patrick J. Fox†

*Golder Associates, 3730 Chamblee Tucker Road, Atlanta, Georgia 30341; and †Department of Civil & Environmental Engineering, University of California, Los Angeles, California 90095
E-mail: yzhu@golder.com

Received August 3, 2001; revised August 13, 2002

A numerical model using smoothed particle hydrodynamics (SPH) for the simulation of pore-scale hydrodynamic dispersion is presented. The model is used to solve the Taylor dispersion problem and explore the characterization of dispersion as an asymptotic Fickian process. Discrete SPH particle data are analyzed using the method of moments. Simulations for pure tracer convection are used to calculate values of tortuosity and effective porosity for two-dimensional spatially periodic porous media. Tracer convection through such media cannot be described as an asymptotic Fickian-type process, even for large times, if the driving body force F is parallel to a line of media symmetry. If F is not parallel to a line of media symmetry, Fickian-type mixing is possible for tracer convection. An asymptotic Fickian approximation is valid for tracer dispersion through two-dimensional spatially periodic porous media when diffusion effects are included.

Key Words: smoothed particle hydrodynamics; convection; diffusion; dispersion; Fickian approximation; porous media.

1. INTRODUCTION

Transport of a nonreacting, nonsorbing dilute tracer in saturated porous media is generally modeled using the convection–dispersion equation [3, 11, 29]

$$\frac{dC}{dt} = \frac{\partial C}{\partial t} + \mathbf{u} \cdot \nabla C = \mathbf{D}\nabla^2 C, \tag{1}$$

where C is tracer concentration, usually defined as mass of tracer per unit volume of solution, t is time, $\mathbf{u}$ is the fluid velocity vector, $\frac{d}{dt}$ is the Lagrangian or material derivative, $\mathbf{D}$ is the hydrodynamic dispersion tensor, and ∇^2 is the Laplacian operator. Equation (1) models

0021-9991/02 $35.00

dispersion in porous media as a diffusional process and predicts that, in a uniform flow field, a set of tracer particles will be normally distributed about a center moving with the average convective velocity [3].

From the viewpoint of classical statistics, if the travel time for an individual tracer particle becomes much larger than the time interval during which successive velocities are positively correlated, its total displacement may be considered as the sum of a large number of elementary displacements that are statistically independent. For such conditions, the probability distribution of the particle's total displacement should be normal according to the central limit theorem [3]. In view of the ergodic principle (i.e., the ensemble averages and time averages are equivalent in an ergodic system), this distribution also represents the spatial distribution of displacements of a cloud of initially close particles. It is this tendency for a cloud of tracer particles to converge to a normal distribution in space and to spread with a variance that is proportional to time that makes it possible to model hydrodynamic dispersion as a diffusional process.

The hydrodynamic dispersion tensor $\mathbf{D}$ is second-rank symmetric and positive definite with principal axes that are generally believed to be oriented parallel and transverse to the mean direction of regional flow [3, 19, 32]. As such, Eq. (1) becomes

$$\frac{\partial C}{\partial t} + \mathbf{u} \cdot \nabla C = D_L \frac{\partial^2 C}{\partial L^2} + D_T \nabla_T^2 C, \tag{2}$$

where D_L is the dispersion coefficient in the direction of the flow L (i.e., the longitudinal dispersion coefficient), D_T is the dispersion coefficient in the direction perpendicular to the flow T (i.e., the transverse dispersion coefficient), and ∇_T^2 is the Laplacian in the transverse directions.

In practice, D_L and D_T are generally expressed in terms of the seepage velocity v_s for an isotropic medium as

$$D_L = d_0 d^* + (a_L v_s)^{m_1}, \tag{3}$$

$$D_T = d_0 d^* + (a_T v_s)^{m_2}, \tag{4}$$

where d_0 is the coefficient of molecular diffusion, d^* is the nondimensional diffusivity of the medium [13, 30, 39], a_L and a_T are the longitudinal and transverse geometrical dispersivities, respectively, for the medium, and m_1 and m_2 are empirical constants between 1 and 2. Laboratory studies have indicated that, for practical purposes, m_1 and m_2 can be generally taken as unity for granular materials [5].

The convection–dispersion equation approach has traditionally considered dispersivity as a characteristic single-valued property of the entire medium [3]. However, several studies have suggested that dispersivity is not a constant but rather depends on the mean travel distance and scale of the problem [12, 14, 21, 31]. Some numerical approaches have been proposed to model scale-dependent dispersion [31, 36]. In the work of Pickens and Grisak [31], dispersivity increases temporally as a function of mean travel distance and approaches an asymptotic value. Tompson [36] described a second-order relationship for local dispersive transport which can be cast in the form of a standard Fickian relationship with time-dependent dispersivity functions that grow to finite, asymptotic values.

To model scale-dependent dispersion, the conventional practice is to simply scale up small dispersivity values observed in column experiments to the much larger values calculated from field trials. However, some of the literature suggests that dispersivity may never

approach an asymptotic finite value for certain cases. As such, the Fickian approximation of dispersion and the traditional convection–dispersion equation are not valid. Matheron and Marsily [24] showed for the special case of a stratified porous medium with flow parallel to bedding that solute transport cannot be generally represented by the convection–dispersion equation, even for large times. Smith and Schwartz [34] concluded that field-scale dispersion (macrodispersion), which is usually caused by mixing due to spatial heterogeneities in the hydraulic conductivity field, cannot be modeled as a large-value diffusion process. Koch and Brady [20] showed that the description of transport in terms of a local, average Fickian process is not applicable if the length and time scales on which a transport process occurs are not much larger than the scale of variations in the velocity field experienced by a tracer particle. Fractal media show long and theoretically infinite correlation scale and the dispersive behavior is inherently pre-asymptotic [10]. In Cushman's nonequilibrium nonlocal theory of transport [10], the concept of classical Fickian dispersive flux is a special case.

Implementations of a numerical solution to the convection–dispersion equation have been realized with the finite difference and finite element methods [4, 37], the method of characteristics [1], and random walk schemes [9]. Mesh-free particle methods, such as the particle strength exchange method [41], provide other interesting alternatives. Pore-scale flow and dispersion has also been simulated using the lattice–Boltzmann technique in which a fluid is modeled according to the average behavior of particles on a lattice rather than as free moving discrete particles [23]. In this paper, hydrodynamic dispersion through two-dimensional spatially periodic porous media is modeled using smoothed particle hydrodynamics (SPH). The work is an extension of that presented by Morris *et al.* [27], Zhu *et al.* [40], and Zhu and Fox [39] and is described in detail by Zhu [38]. Section 2 presents the SPH model and the method of moments used to interpret simulation results. In Section 3, the model is verified by simulating the classical Taylor dispersion problem. In Section 4, the SPH model is used to simulate purely convective transport (i.e., without diffusion effects). In Section 5, diffusion is included in the SPH model to simulate hydrodynamic dispersion. The dispersion properties of spatially periodic porous media are calculated and the validity of the asymptotic Fickian assumption for the description of the hydrodynamic dispersion of a tracer at the pore-scale level is investigated. Section 6 presents conclusions of the study along with a discussion of the strengths and weaknesses of the SPH dispersion model.

2. SPH MODEL FOR HYDRODYNAMIC DISPERSION

Smoothed particle hydrodynamics was originally developed for astrophysical applications to model compressible fluids at high Reynolds number [15, 22]. SPH is a fully Lagrangian computational fluid dynamics technique in which the numerical solution is achieved without a grid. The standard approach to SPH is reviewed by Benz [6] and Monaghan [25]. In SPH, a compressible fluid is represented by a field of disordered particles (Fig. 1), typically of fixed mass, which follow the local fluid motion, convect contact discontinuities, preserve Galilean invariance, and reduce computational diffusion of various fluid properties including momentum when compared to the finite difference method. The equations governing the evolution of the fluid become expressions for interparticle forces and fluxes when written in SPH form. In standard SPH, each particle carries mass m, density ρ, velocity $\mathbf{u}$, and other fluid quantities specific to a given problem. Each particle is

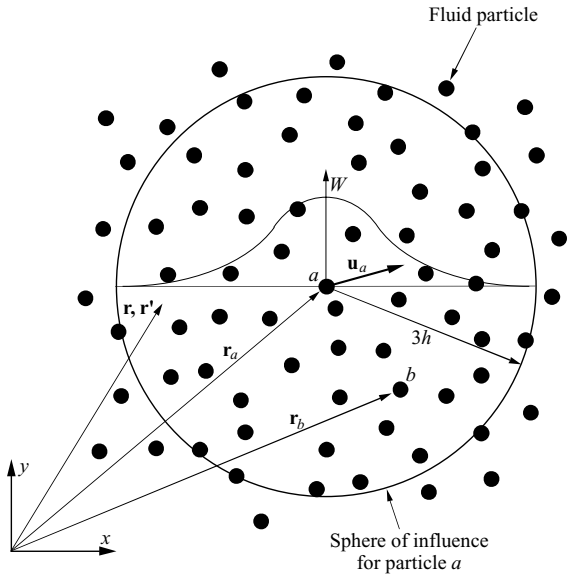

FIG. 1. Sphere of influence for SPH particle a.

mathematically treated as an interpolation point at which fluid properties are computed as the weighted sum of values from neighboring particles.

2.1. Evolution of Flow Field

Water flow through porous media is generally regarded as incompressible since the bulk fluid velocity is much smaller than the corresponding speed of sound. The solution to an incompressible flow problem is achieved by solving the mass and momentum conservation equations throughout the flow domain subjected to proper boundary conditions,

$$\nabla \cdot \mathbf{u} = 0, \tag{5}$$

$$\frac{d\mathbf{u}}{dt} = -\frac{1}{\rho}\nabla p + \nu\nabla^2\mathbf{u} + \mathbf{g}, \tag{6}$$

where p is pressure, ν is the fluid kinematic viscosity, and $\mathbf{g}$ is gravitational acceleration.

SPH was recently extended to model low-Reynolds-number ($Re \leq 1$) incompressible flow [27, 40]. A brief overview of the method used to evaluate fluid particle accelerations for quasi-incompressible viscous flows is provided here. Readers are referred to Morris *et al.* [27] and Zhu *et al.* [40] for other modifications to the standard SPH formalism that are needed to minimize errors for simulating such flows.

In SPH, the pressure gradient acceleration term is usually symmetrized by writing

$$\frac{\nabla p}{\rho} = \nabla\left(\frac{p}{\rho}\right) + \frac{p}{\rho^2}\nabla\rho. \tag{7}$$

This results in the most common SPH expression for the term

$$-\left(\frac{1}{\rho}\nabla p\right)_a = -\sum_b m_b\left(\frac{p_a}{\rho_a^2} + \frac{p_b}{\rho_b^2}\right)\nabla_a W_{ab}, \tag{8}$$

where W is the SPH kernel function, subscripts a and b denote SPH particles a and b, respectively, and ∇_a denotes the gradient with respect to coordinates of particle a. The kernel typically takes the form

$$W(\mathbf{r}, h) = \frac{1}{h^\sigma} f\left(\frac{|\mathbf{r}|}{h}\right), \tag{9}$$

where σ is the number of dimensions for the problem, h is the smoothing length, $W_{ab} = W(\mathbf{r}_{ab}, h)$, and $\mathbf{r}_{ab} = \mathbf{r}_a - \mathbf{r}_b$. Provided that the SPH kernel is an even function of $\mathbf{r}$, Eq. (8) conserves linear and angular momenta exactly since the forces acting between individual particles are antisymmetric. Momentum conservation can be satisfied by an infinite number of symmetric forms of the pressure gradient acceleration term given by Monaghan [25],

$$-\left(\frac{1}{\rho}\nabla p\right)_a = -\sum_b m_b \left(\frac{p_a}{\rho_a^\varepsilon \rho_b^{2-\varepsilon}} + \frac{p_b}{\rho_b^\varepsilon \rho_a^{2-\varepsilon}}\right)\nabla_a W_{ab}, \tag{10}$$

where ε may take any value. The form (i.e., $\varepsilon = 1$)

$$-\left(\frac{1}{\rho}\nabla p\right)_a = -\sum_b m_b \left(\frac{p_a + p_b}{\rho_a \rho_b}\right)\nabla_a W_{ab} \tag{11}$$

provides certain advantages for problems involving contact discontinuities and was used for the study described herein.

Many forms of artificial viscosity have been proposed for modeling viscous fluid in SPH [6, 25]. The current method employed an SPH estimation of viscous diffusion as [27, 40]

$$(\nu\nabla^2\mathbf{u})_a = \left(\frac{\mu}{\rho}\nabla^2\mathbf{u}\right)_a = \sum_b \frac{m_b(\mu_a + \mu_b)\mathbf{r}_{ab}\cdot\nabla_a W_{ab}}{\rho_a\rho_b\left(\mathbf{r}_{ab}^2 + 0.01\,h^2\right)}\mathbf{u}_{ab}, \tag{12}$$

where μ is fluid dynamic viscosity, $\mathbf{u}_{ab} = \mathbf{u}_a - \mathbf{u}_b$, and the $0.01\,h^2$ term is included to maintain a nonzero denominator. Equation (12) is based on a similar SPH expression used by Monaghan [26] to model heat conduction. This hybrid expression combines a standard SPH first derivative with a finite difference approximation of a first derivative. By taking a Taylor expansion about particle a, it can be shown that this expression is approximate since it conserves linear momentum exactly, while angular momentum is only approximately conserved [26].

Based on the SPH evaluations of pressure gradient acceleration and viscous diffusion, momentum conservation is written as

$$\frac{d\mathbf{u}_a}{dt} = -\sum_b m_b\left(\frac{p_a + p_b}{\rho_a\rho_b}\right)\nabla_a W_{ab} + \sum_b \frac{m_b(\mu_a + \mu_b)\mathbf{u}_{ab}}{\rho_a\rho_b}\left(\frac{1}{|\mathbf{r}_{ab}|}\frac{\partial W_{ab}}{\partial r_{ab}}\right) + \mathbf{g}, \tag{13}$$

and mass conservation is expressed as

$$\frac{d\rho_a}{dt} = \sum_b m_b \mathbf{u}_{ab}\cdot\nabla_a W_{ab}. \tag{14}$$

A state equation relates particle pressure and density as

$$p_a = c^2\rho_a, \tag{15}$$

where c is the speed of sound chosen to ensure that the particle densities vary no more than approximately 1%.

No-slip boundary conditions are implemented to simulate flow in porous media [27]. Simulations using the method show close agreement with series solutions for Couette and Poiseuille flows [27]. Furthermore, comparison with finite element solutions for flow past a regular lattice of cylinders shows close agreement for the velocity and pressure fields [40].

2.2. Evolution of Tracer Diffusion

The solution for tracer diffusion (i.e., diffusion of a nonreacting, nonsorbing species within a stationary fluid) in porous media is achieved by solving the following diffusion equation subjected to proper boundary conditions:

$$\frac{dC}{dt} = d_0 \nabla^2 C. \tag{16}$$

If the diffusion equation is rewritten as

$$\frac{dC}{dt} = d_0 \nabla^2 C = \frac{d_0 \rho}{\rho} \nabla^2 C, \tag{17}$$

it becomes evident that the method used to treat viscosity (Eq. (12)) can be adopted to evolve tracer concentration [39],

$$\frac{dC_a}{dt} = \left(\frac{d_0 \rho}{\rho} \nabla^2 C \right)_a = \sum_b \frac{m_b (d_{0,a} \rho_a + d_{0,b} \rho_b) \mathbf{r}_{ab} \cdot \nabla_a W_{ab}}{\rho_a \rho_b \left(\mathbf{r}_{ab}^2 + 0.01\, h^2 \right)} C_{ab}, \tag{18}$$

where $C_{ab} = C_a - C_b$. Comparative studies with available analytical and numerical solutions show that the SPH diffusion model has excellent accuracy and that the accuracy increases with increasing numerical resolution for a given problem [39].

2.3. Hydrodynamic Dispersion in Periodic Porous Media

The SPH hydrodynamic dispersion model was developed by implementing both fluid flow and diffusion simultaneously within a simulation. As such, SPH particles move in response to local pressure gradients and tracer mass diffuses from particle to particle in response to local concentration gradients. Particle positions and concentrations are updated using a predictor–corrector technique in which the time step is limited by appropriate stability constraints [27, 38, 39].

The model has been used to simulate hydrodynamic dispersion in spatially periodic porous media that are generated by repeating unit cells in one, two, or three dimensions. In spatially periodic porous media, while the low-Reynolds-number flow field is also periodic in nature, this is not true for the concentration field. As a result, a computing domain consisting of multiple unit cells is needed to evolve the concentration field. Figure 2 shows the initial concentration field for a problem of tracer dispersion. The concentration computing domain consists of six unit cells identified by (i, j) coordinates. For this tracer hydrodynamic dispersion model, the flow field is calculated for a single unit cell corresponding to $i = 1$ and $j = 1$. Every SPH fluid particle has one set of flow-related quantities (e.g., velocity and density) and carries one concentration value for each unit cell in the concentration-computing domain. In this case, each fluid particle carries six values of concentration. The

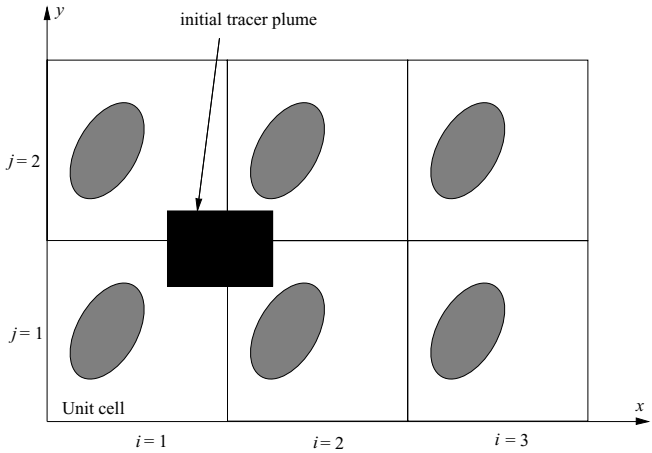

FIG. 2. Initial concentration field for a problem of tracer hydrodynamic dispersion in a spatially periodic porous medium.

concentration field is determined by the particle concentration values for each unit cell. However, particle positions in unit cell (i, j) other than unit cell (1, 1) are not needed during the course of a simulation since the evolution of concentration field is driven by local concentration gradients and only the relative positions between particles are needed. These positions are calculated from unit cell (1, 1) and are the same for every unit cell. For the purpose of analyzing and visualizing the concentration field, SPH particles are mapped to other unit cells in the concentration-computing domain from unit cell (1, 1).

To perform the simulation in Fig. 2, the flow field is evolved to steady state with all particle concentrations equal to zero. Particles in area A (Fig. 3) are then assigned a concentration value of unity for unit cell (1, 1) and particles in areas B, C, and D are assigned concentration values of unity for unit cells (1, 2), (2, 2), and (2, 1), respectively. Once the concentration field is initialized, the flow continues according to the method described in Section 2.1 and the concentration field is evolved according to the method described in Section 2.2. Although the tracer field is initially represented by a certain number of fluid particles (the

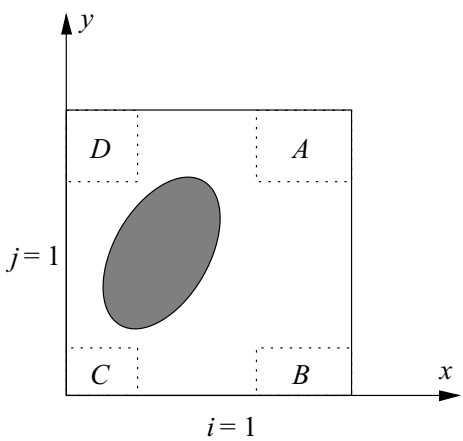

FIG. 3. Unit cell (1, 1) for the problem in Fig. 2.

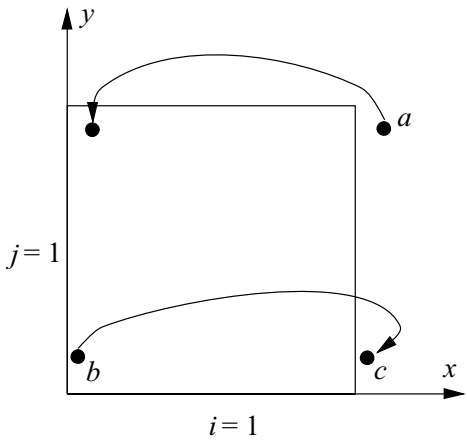

FIG. 4. Wrapping fluid particles and creating image particles to simulate tracer dispersion in a spatially periodic porous medium.

initial tracer particles), every fluid particle has the potential to carry solute mass later in a simulation due to diffusion. Because fluid particles are wrapped around the unit cell (1, 1) and all SPH particles physically reside inside unit cell (1, 1), concentration values of the wrapped particles are reassigned accordingly. For example, as fluid particle a (Fig. 4) is wrapped back into unit cell (1, 1), its value of concentration for unit cell (i, j) after wrapping is equal to its value of concentration for unit cell $(i - 1, j)$ before wrapping.

Values of concentration must also be correctly assigned to image fluid particles needed for proper implementation of boundary conditions in the SPH method [27, 38]. For example, if particle c is the image particle of particle b in unit cell (1, 1) (Fig. 4), the value of concentration for particle c corresponding to unit cell (i, j) is equal to the value of concentration for particle b corresponding to unit cell $(i + 1, j)$.

The concentration-computing domain used in this work consisted of a constant number of unit cells. Each simulation was terminated when the tracer field crossed the boundary of the domain. Although a large concentration-computing domain (e.g., column $i = 3$ in Fig. 2) may be unnecessary during the initial stages of a simulation, several tens of unit cells are usually needed for a meaningful simulation of hydrodynamic dispersion as the tracer field spreads out. The computing efficiencies gained by dynamically changing the size of the concentration-computing domain during the course of a simulation are not explored in this work. Readers are referred to Morris *et al.* [28] for information on the computation time requirements of the flow simulation method.

If $d_0 = 0$, particle-to-particle diffusion does not occur and pure tracer convection is simulated. As there is no mass exchange between tracer and carrier fluid for pure tracer convection, the solute mass associated with each initial tracer particle is constant during the course of a simulation. Thus, initial tracer and fluid particles can be simply distinguished as "black" and "white" fluid particles, respectively, for this case.

2.4. Method of Moments

Evaluation of spatial moments of the tracer distribution can provide an estimation of the dispersivity of porous media [2, 7, 16]. For the SPH hydrodynamic dispersion model,

each fluid particle is characterized by position $\mathbf{R}$ and solute mass $\mathcal{M} = Cm/\rho$. The zeroth moment M_0, first moment $\mathbf{M}_1$, and centered second moment $\mathbf{M}_2$ of tracer distribution are, respectively,

$$M_0 = \frac{\int d\mathcal{M}}{\int d\mathcal{M}_o} = \frac{\int C dV}{\int C_o\, dV} \cong \frac{\sum_b C_b \frac{m_b}{\rho_b}}{\sum_b C_{b,o} \frac{m_b}{\rho_{b,o}}}, \tag{19}$$

$$\mathbf{M}_1 = \frac{\int \mathbf{R} d\mathcal{M}}{\int d\mathcal{M}_o} = \frac{\int \mathbf{R} C dV}{\int C_o\, dV} \cong \frac{\sum_b \mathbf{R}_b C_b \frac{m_b}{\rho_b}}{\sum_b C_{b,o} \frac{m_b}{\rho_{b,o}}}, \tag{20}$$

and

$$\mathbf{M}_2 = \frac{\int (\mathbf{R} - \mathbf{M}_1)^2\, d\mathcal{M}}{\int d\mathcal{M}_o} = \frac{\int (\mathbf{R} - \mathbf{M}_1)^2\, C dV}{\int C_o\, dV} \cong \frac{\sum_b (\mathbf{R}_b - \mathbf{M}_1)^2\, C_b \frac{m_b}{\rho_b}}{\sum_b C_{b,o} \frac{m_b}{\rho_{b,o}}}, \tag{21}$$

where summations are performed over all fluid particles and subscript o denotes an initial value. M_0 will have a constant value of unity if tracer mass is conserved during a simulation. $\mathbf{M}_1$ represents the position of the center of tracer mass and is used to calculate the seepage velocity $\mathbf{v}_s$ as

$$\mathbf{v}_s = \frac{\Delta \mathbf{M}_1}{\Delta t}. \tag{22}$$

$\mathbf{M}_2$ represents the spreading of a tracer field about its center and is used to calculate the dispersion coefficient as

$$\mathbf{D} = \frac{\Delta \mathbf{M}_2}{2\Delta t}. \tag{23}$$

Zhu [38] showed that for tracer diffusion through porous media the method of moments produces reliable values for the effective diffusion coefficient when compared with corresponding values obtained from steady-state diffusion simulations. In the latter approach, a concentration difference is applied across the unit cell of a periodic porous medium and the resulting concentration field at steady state is used to obtain the effective diffusion coefficient of the medium [39].

3. SIMULATIONS OF TAYLOR DISPERSION

Dispersion of a tracer in a fluid flowing between stationary infinite plates at $y = 0$ and $y = L$ (Fig. 5) was simulated using the SPH hydrodynamic dispersion model. The method of moments was employed to yield values of Taylor dispersion coefficient D_{Taylor}, which were compared with values from the analytical solution [17, 18]

$$D_{\text{Taylor}} = d_0 + \frac{L^2 v_s^2}{210\, d_0}, \tag{24}$$

where v_s is the average fluid velocity determined by

$$v_s = \frac{F L^2}{12 \nu} \tag{25}$$

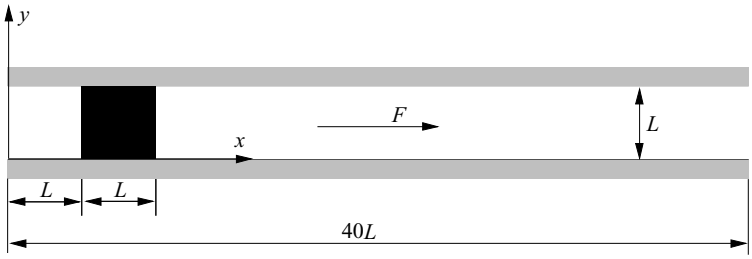

FIG. 5. Initial condition ($t = 0$) for Taylor dispersion between parallel plates. Tracer particles (shown in black) have an initial concentration of unity.

and F is the body force driving the flow. Equation (24) is based on Taylor's original solution for hydrodynamic dispersion in a cylindrical tube [35]. To observe asymptotic behavior, t must evolve to a value greater than t_c, which is defined for this problem geometry as

$$t_c = \frac{L^2}{4d_0}. \tag{26}$$

Time t_c is the characteristic time for transverse diffusion in the Taylor dispersion problem.

SPH was used to simulate dispersion for $L = 0.001$ m; $\rho = 10^3$ kg/m^3; $\nu = 10^{-6}$ m^2/s; $d_0 = 10^{-6}$ m^2/s; $F = 0.05, 0.10$, and 0.15 m/s^2; and 50 fluid particles spanning the distance L. After the flow was evolved to steady Poiseuille conditions, dispersion simulations began with the initial tracer configuration shown in Fig. 5. Figure 6 shows two plots of the tracer concentration field generated from the discrete fluid particle data for $F = 0.10$ m/s^2.

The three Taylor dispersion simulations showed that tracer mass was conserved ($M_0 \cong 1$) in each case. Figure 7 is a plot of first moment in the x-direction M_{1x} as a function of time. Values of M_{1x} were computed by subtracting the first moment at time $t = 0$ from those at

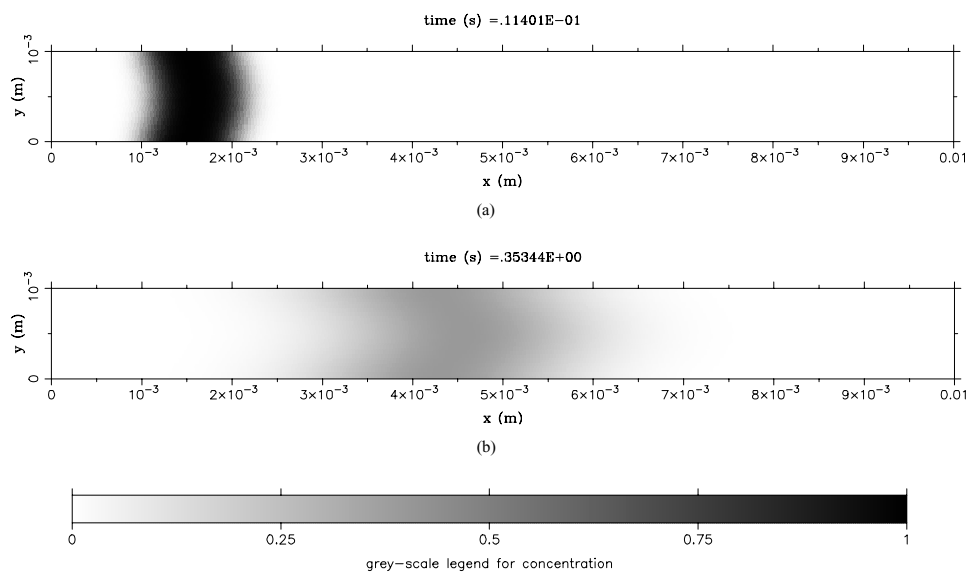

FIG. 6. Tracer concentration fields for Taylor dispersion between parallel plates at (a) $t = 0.01140$ s, and (b) $t = 0.35344$ s.

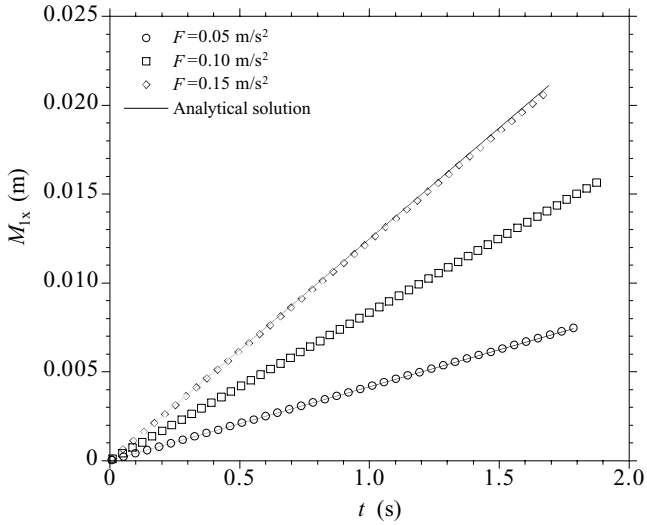

FIG. 7. First moment in the x-direction of tracer concentration versus time for Taylor dispersion between parallel plates.

time t. Figure 7 shows that the center of tracer mass moved at constant velocity in each case. Values of average fluid velocity v_s (Eq. (22)) differ from the analytical solutions by a maximum of 1.2%.

Figure 8 is a plot of centered second moment in the x-direction M_{2x} as a function of time. Values of M_{2x} were computed by subtracting centered second moment at time $t = t_c$ from those at time t. Figure 8 shows that, in each case, tracer spreading about its center grows linearly with time for $t > t_c$. The corresponding asymptotic values of dispersion coefficient in the x-direction D_{Taylor} (Eq. (23)) are 1.06×10^{-6}, 1.30×10^{-6}, and 1.68×10^{-6} m^2/s

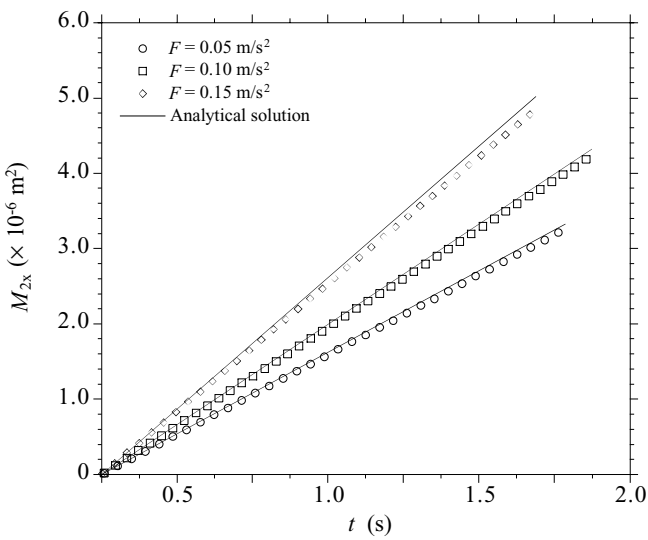

FIG. 8. Centered second moment in the x-direction of tracer concentration versus time for Taylor dispersion between parallel plates.

for $F = 0.05$, 0.10, and 0.15 m/s^2, respectively. SPH solutions for D_{Taylor} were less than the analytical solutions by a maximum of 3.4%.

4. SIMULATIONS OF TRACER CONVECTION

Five simulations were completed for tracer convection (i.e., without particle-to-particle diffusion) through spatially periodic porous media with circular cylinders arranged in square, staggered, and hexagonal arrays. Each medium has a porosity $n = 0.8$ and a cylinder radius $R = 0.5$ mm. The fluid was modeled as water (i.e., $\rho = 10^3$ kg/m^3 and $\nu = 10^{-6}$ m^2/s) driven by body force F. The direction of F is denoted by L, the direction perpendicular to F is denoted by T, and the angle between F and the x-axis is denoted by γ (Fig. 9). Figures 10–14 show tracer particle fields at certain values of t for the five simulations. The tracer fields were analyzed using the method of moments for seepage velocity v_s, effective porosity n_{eff}, and mechanical dispersion coefficients D_{mL} and D_{mT}. Tortuosity $\mathcal{T}$ of each medium was also calculated. Table I presents a summary of results for the tracer convection simulations, where N_{part} denotes the total number of SPH particles per unit cell for each simulation.

4.1. Tortuosity of Porous Media

Figures 15 and 16 show the pathlines of four tracer particles for the hexagonal array simulations. Each particle takes a tortuous path to avoid obstacles (i.e., solid grains) in the flow field. Values of tortuosity $\mathcal{T}$ for the porous media were calculated as

$$\mathcal{T} = \frac{\sum_z \frac{L_{e,z}}{L_z}}{N_{\text{tracer}}}, \tag{27}$$

where $L_{e,z}$ and L_z are lengths of the pathline and straight-line distances traveled by tracer particle z, respectively (Fig. 17), and N_{tracer} is the total number of tracer particles in the flow field.

Figure 18 shows the tortuosity of the media as a function of time for each tracer convection simulation. A constant tortuosity value is reached in each case for $t > 200$ s. Tortuosity values for the five simulations are considerably less than the commonly used value of $\sqrt{2} = 1.414$ proposed by Carman [8] for unconsolidated porous aggregates. It is also apparent that tortuosity is a function of media geometry. For the three simulations with $\gamma = 0^\circ$, the square and staggered arrays have the smallest and largest tortuosity values, respectively. For the square array with $\gamma = 0^\circ$, most of the tracer particles have an unobstructed travel

TABLE I
Summary of Results for Five Tracer Convection Simulations

Simulation	Array type	N_{part}	F (m/s^2)	γ	$\mathcal{T}$	v_s (m/s)	v (m/s)	Re	n_{eff}
1	square	3384	0.001	0°	1.051	9.30×10^{-5}	7.35×10^{-5}	0.047	0.790
2	staggered	8320	0.001	0°	1.139	9.06×10^{-5}	7.17×10^{-5}	0.045	0.791
3	staggered	8320	0.001	30°	1.067	9.08×10^{-5}	7.18×10^{-5}	0.045	0.791
4	hexagonal	8160	0.0007	0°	1.094	6.57×10^{-5}	5.19×10^{-5}	0.033	0.790
5	hexagonal	8160	0.0007	45°	1.082	6.56×10^{-5}	5.18×10^{-5}	0.033	0.790

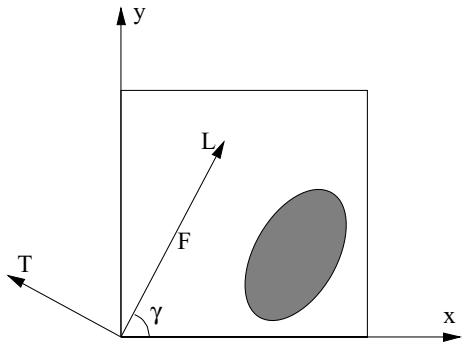

FIG. 9. Body force F with direction L and perpendicular direction T.

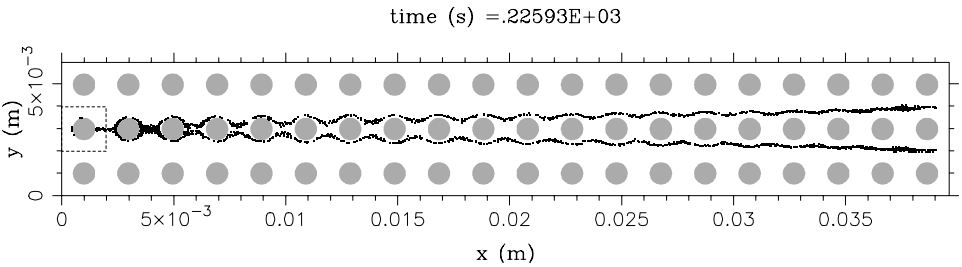

FIG. 10. Tracer convection through a square array of circular cylinders ($\gamma = 0°$). Tracer particles (shown in black) initially occupied the area enclosed by the dashed box.

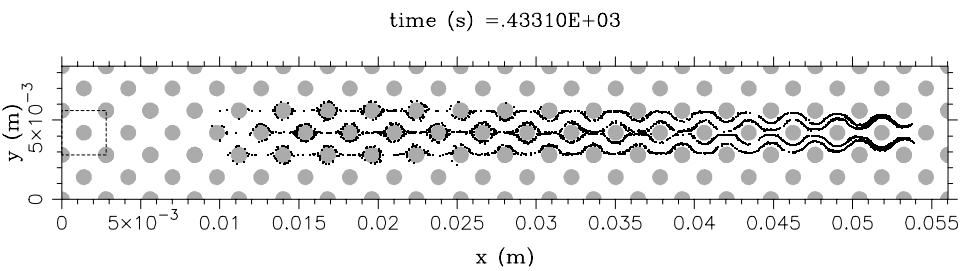

FIG. 11. Tracer convection through a staggered array of circular cylinders ($\gamma = 0°$). Tracer particles (shown in black) initially occupied the area enclosed by the dashed box.

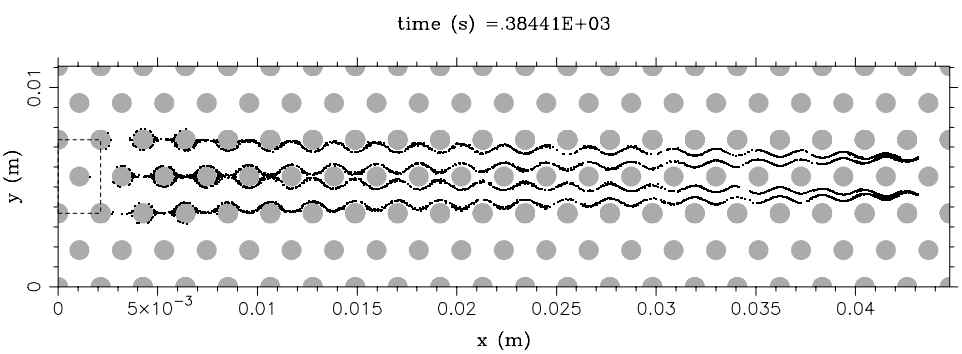

FIG. 12. Tracer convection through a hexagonal array of circular cylinders ($\gamma = 0°$). Tracer particles (shown in black) initially occupied the area enclosed by the dashed box.

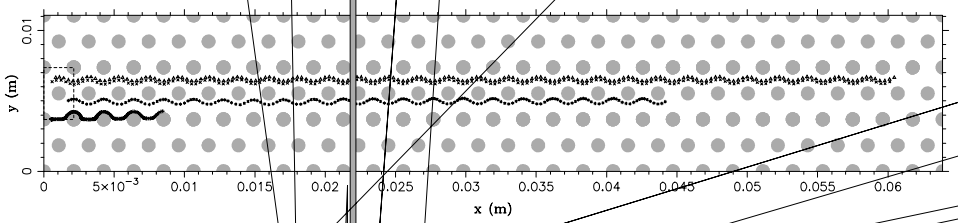

FIG. 15. Pathlines of four tracer particles in a hexagonal array of circular cylinders ($\gamma = 0^\circ$).

and straight-line distance

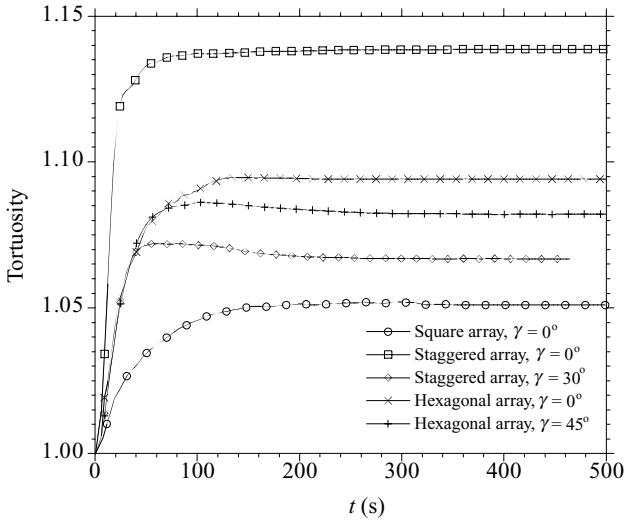

FIG. 18. Tortuosity versus time for five simulations of tracer convection.

path, which produces a tortuosity value close to unity. The staggered array introduces more obstacles into the flow field and tortuosity increases as a result. Although the hexagonal array has the same solid surface area per unit cell as the staggered array, it has larger flow channels, which results in a tortuosity value intermediate between those for the square and staggered arrays.

Not only is tortuosity a function of media geometry, it is also a function of the direction of the applied body force. The effect of body force direction on tortuosity is apparent for the staggered array simulations. For $\gamma = 30^\circ$, fewer tracer particles must travel around the center solid grain in the staggered array than for $\gamma = 0^\circ$. This results in a lower tortuosity value for $\gamma = 30^\circ$. Similar observations can be made regarding the effect of γ for the hexagonal array.

4.2. Seepage Velocity and Effective Porosity of Porous Media

Seepage velocity for each tracer convection simulation was calculated using Eq. (22). The seepage velocity in the L-direction v_{sL} fluctuates within a 5% range about an average value of v_s for each simulation, which indicates that the tracer flow field is numerically stable. Values of v_s (Table I) were used to calculate Reynolds number $Re = v_s R/\nu$ for the simulations. The small values of Re indicate creeping flow conditions.

The value of effective porosity n_{eff} for each medium (Table I) was calculated as

$$n_{\text{eff}} = \frac{v}{v_s}, \tag{28}$$

where v is the steady-state Darcy velocity in the L-direction. The effective porosity excludes "dead-end" pores and thus represents the fraction of pore space that is available to transmit fluids. For the media type considered in this work, n_{eff} should be equal to n. The small difference between n_{eff} and n in Table I may be due to the placement of SPH boundary particles [38]. As the first layer of boundary particles is placed on the solid surface, the porous medium simulated actually has a porosity slightly smaller than the nominal value. Although n_{eff} is nearly equal to n for uniform granular materials, it may be significantly

less than n for clays due to their more complex microfabric of clay particle clusters and intercluster voids [33].

4.3. Mechanical Dispersion Coefficients of Porous Media

Mechanical dispersion coefficients for tracer convection were calculated using Eq. (23). Figures 19 and 20 show M_{2L}, M_{2T}, D_{mL}, and D_{mT} as functions of time for the simulations 1 to 4 (Table I). M_{2L}, M_{2T}, D_{mL}, and D_{mT} denote centered second moments and mechanical dispersion coefficients in the L- and T-directions, respectively. Values of M_{2L} and M_{2T} were computed by subtracting centered second moments at time $t = 0$ from those at time t.

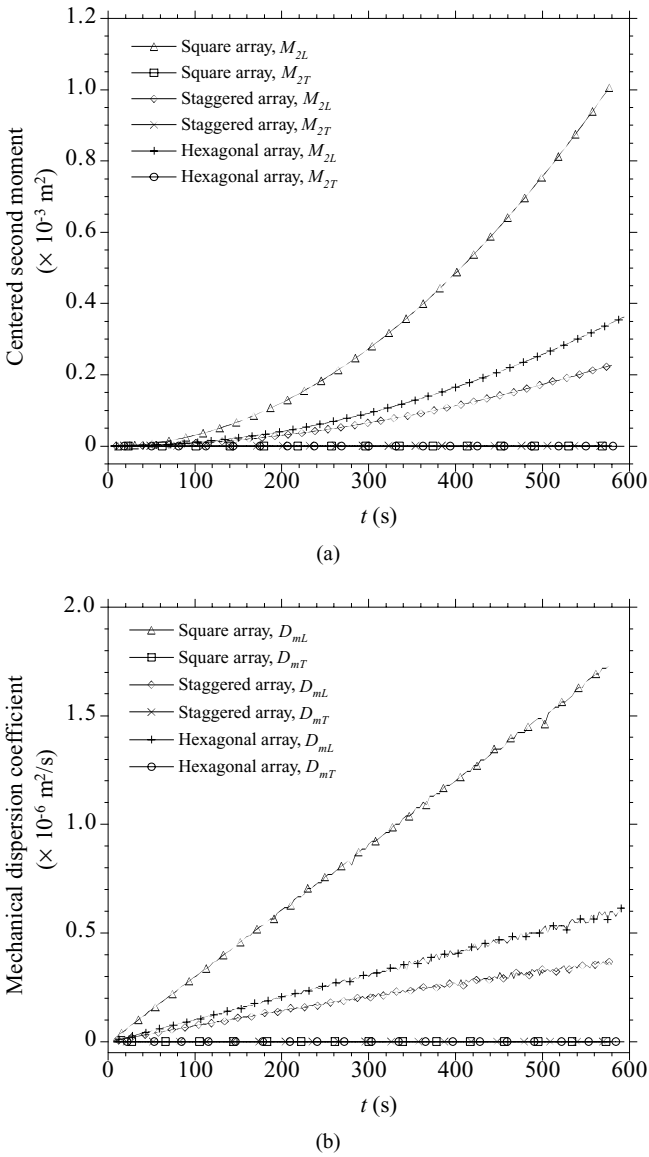

FIG. 19. (a) Centered second moment and (b) mechanical dispersion coefficient versus time for tracer convection through square, staggered, and hexagonal arrays of circular cylinders ($\gamma = 0°$).

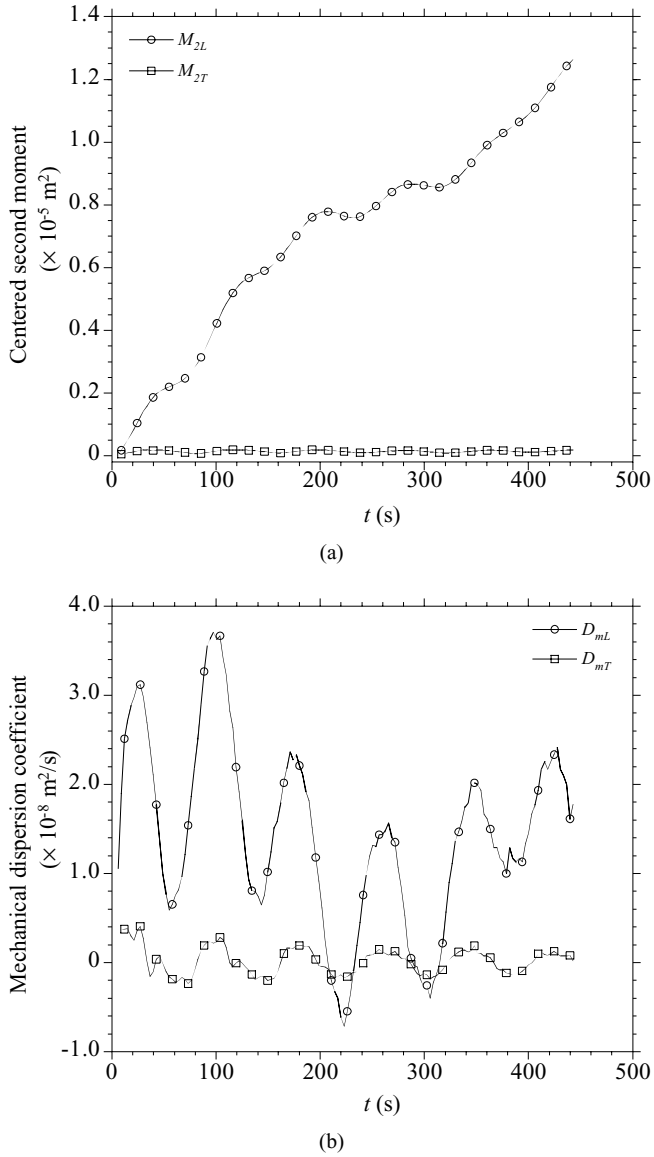

FIG. 20. (a) Centered second moment and (b) mechanical dispersion coefficient versus time for tracer convection through a staggered array of circular cylinders ($\gamma = 30^\circ$).

M_{2L} and D_{mL} show different characteristics depending on the body force direction. When F is parallel to a line of symmetry of the solid inclusions, periodic pathlines exist, M_{2L} increases nearly quadratically with t and D_{mL} increases nearly linearly with t (Fig. 19). When F is not parallel to a line of symmetry of the solid inclusions, irregular pathlines exist and M_{2L} shows a more irregular behavior (Fig. 20). Although M_{2L} generally increases with t in this case, it may decrease for short periods, which results in a negative value of D_{mL}. Figure 20 b shows that D_{mL} does not steadily increase with time and instead fluctuates about an average value. When F is parallel to a line of media symmetry, M_{2T} and D_{mT} are practically zero (Fig. 19). When F is not parallel to a line of media symmetry, M_{2T}

shows small fluctuations about zero, which are amplified when D_{mT} is calculated (Fig. 20). Results for simulation 5 (Table I) show characteristics similar to those of simulation 4 [38].

Cushman [10] expressed the relationship between centered second moment and time as

$$\log(M_2) = s \log(t). \tag{29}$$

A value of $s = 1$ corresponds to a Fickian behavior. An evaluation of the simulation data shows that an approximately linear relationship exists between $\log(M_{2L})$ and $\log(t)$ in each case [38]. If F is parallel to a line of media symmetry, the linear fits for M_{2L} are quite good and $s \cong 2$. When F is not parallel to a line of media symmetry, s has a value close to unity, which suggests an approximate Fickian dispersion behavior.

An asymptotic mechanical dispersion coefficient was not found for two-dimensional tracer convection through spatially periodic porous media when F is parallel to a line of media symmetry, even for large times. Constant dispersivity implies that a single velocity path is statistically representative of all velocity paths. This means that a tracer particle released anywhere in the unit cell of a spatially periodic porous medium will eventually sample the entire unit cell by convection alone. However, when F is parallel to a line of media symmetry (e.g., Fig. 15), different tracer particles experience consistently different velocity paths. In this case, spatially periodic pathlines are apparent and the velocity of a tracer particle remains correlated with the media structure throughout all space. The distance between two tracer particles released on different streamlines increases with time, seemingly without bound.

Figure 16 shows particle pathlines for a case in which F is not parallel to a line of media symmetry. Although pathlines do not cross each other under laminar flow conditions, irregular pathlines allow tracer particles to sample velocity fields throughout the unit cell during the course of a simulation. This results in a mixing process which can be approximated as Fickian. Figure 21 illustrates this concept. In Fig. 21a, F is parallel to a line of media symmetry and the tracer particles always sample the same velocity path throughout the simulation; in Fig. 21b, F is not parallel to a line of media symmetry and the tracer particles eventually sample the velocity field of the entire unit cell. Another mechanism which allows tracer mass to sample the velocity field of the entire unit cell is molecular diffusion. The following section discusses this issue.

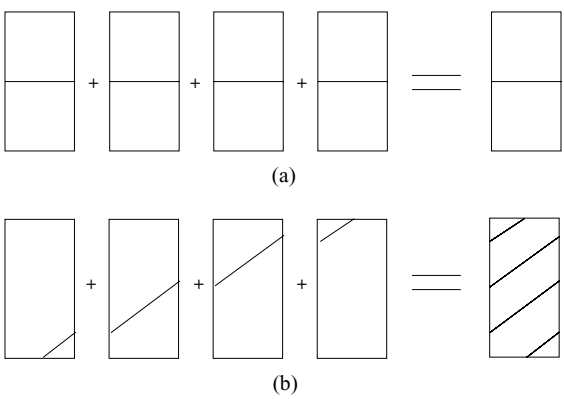

FIG. 21. Pathlines of tracer particles when (a) F is parallel to a line of media symmetry and (b) F is not parallel to a line of media symmetry.

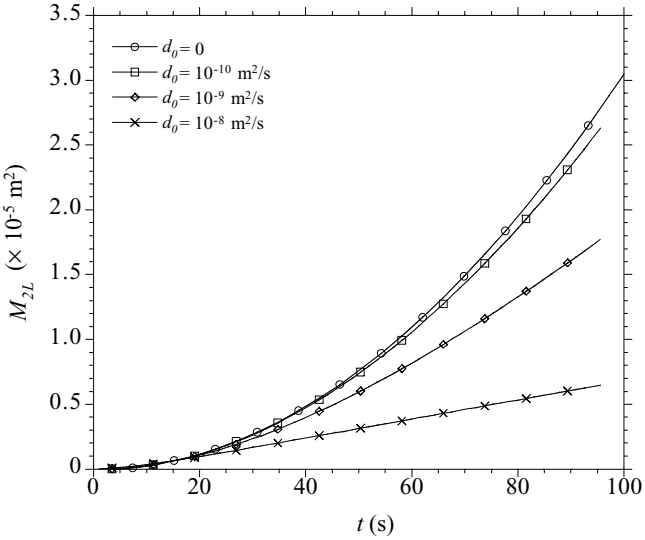

FIG. 23. Centered second moment in the L-direction versus time for one-dimensional tracer transport through a square array of circular cylinders.

asymptotic Fickian behavior exists for tracer hydrodynamic dispersion under this condition. However, this behavior appears some time after the tracer is introduced into the flow. A characteristic time t_c defined as [7]

$$t_c = \frac{\mathcal{L}_D^2}{d_0} \tag{30}$$

is required for a tracer to sample all interstitial space of the unit cells, where $\mathcal{L}_D$ is the

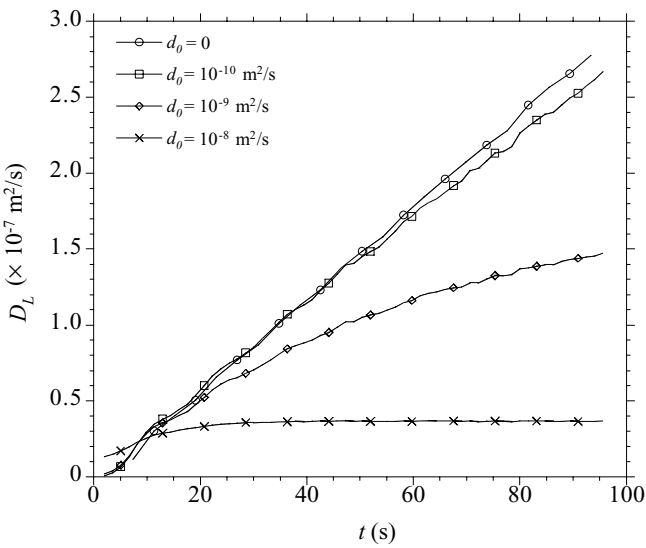

FIG. 24. Dispersion coefficient in the L-direction versus time for one-dimensional tracer transport through a square array of circular cylinders.

characteristic Darcy length scale of the medium. The value of d_0 directly controls the value of t_c and hence the process that tracer particles sample pore spaces through molecular diffusion. If $\mathcal{L}_D = R = 0.5$ mm, $t_c = 25$ s for the simulation with $d_0 = 10^{-8}$ m^2/s. This is approximately the time at which D_L becomes essentially constant in Fig. 24. However, $t_c = 2500$ s for $d_0 = 10^{-10}$ m^2/s and $t_c = 250$ s for $d_0 = 10^{-9}$ m^2/s. Due to the small time step limited by fluid viscosity and a large concentration-computing domain, these simulations could not be run long enough to reach their t_c values.

6. CONCLUSIONS

A pore-scale hydrodynamic dispersion model was developed using smoothed particle hydrodynamics. The model was used to simulate Taylor dispersion and the results were in close agreement with analytical solutions. Simulations corresponding to pure tracer convection (i.e., with no particle-to-particle diffusion) were used to calculate tortuosity and effective porosity for three spatially periodic configurations of two-dimensional porous media. It was found that pure tracer convection cannot be described as an asymptotic Fickian-type process, even for large times, if the driving body force F is parallel to a line of media symmetry. If F is not parallel to a line of media symmetry, Fickian-type mixing is possible for pure tracer convection. An asymptotic Fickian approximation is also valid for tracer hydrodynamic dispersion (i.e., including particle-to-particle diffusion) after a certain characteristic time that decreases with increasing value of molecular diffusion coefficient.

As a mesh-free particle method, SPH can incorporate the physics of flow and mass transport to simulate hydrodynamic dispersion at the pore-scale level. The method can also be used to systematically study dispersion phenomena as a function of media properties and flow conditions. A clear advantage of the approach is that the Lagrangian framework of SPH allows the effects of convection-driven mechanical mixing to be evaluated separately from the effects of particle-to-particle diffusion. The mesh-free character of SPH and the straightforward physical interpretation of the results make this an attractive alternative to established methods such as finite differences or finite elements. Computational cost remains a limitation of the method for pore-scale modeling of hydrodynamic dispersion due to numerical stability constraints of the time step. Although periodic boundaries were used to reduce the flow computations to those of a single unit cell in this study, a meaningful simulation of hydrodynamic dispersion in periodic porous media required several tens of unit cells for modeling the evolution of a concentration field. Combined with the need for longer simulated flow times to achieve asymptotic dispersive behavior, this significantly lengthened the computation time for each simulation (up to several weeks).

ACKNOWLEDGMENTS

The authors extend their sincere thanks to Dr. Joseph P. Morris of Lawrence Livermore National Laboratory for many insightful discussions regarding the use of SPH to model dispersion. This work was sponsored by the Air Force Office of Scientific Research, USAF, under Grant F49620-96-1-0020. The views and conclusions contained herein are those of the authors and should not be interpreted as necessarily representing the official policies or endorsements, either expressed or implied, of the Air Force Office of Scientific Research or the U.S. Government.

REFERENCES

1. M. B. Abbott, *An Introduction to the Method of Characteristics* (American Elsevier, New York, 1966).
2. R. Aris, On the dispersion of a solute in a fluid flowing through a tube, *Philos. Trans. R. Soc. London Ser. A* **235**, 67 (1956).
3. J. Bear, *Dynamics of Fluids in Porous Media* (American Elsevier, New York, 1972).
4. J. Bear and A. Verruijt, *Modeling Groundwater Flow and Pollution* (Reidel, New York, 1987).
5. P. B. Bedient, H. S. Rifai, and C. J. Newell, *Ground Water Contamination: Transport and Remediation* (Prentice Hall, Englewood Cliffs, NJ, 1994).
6. W. Benz, Smooth particle hydrodynamics: A review, in *The Numerical Modelling of Nonlinear Stellar Pulsations*, edited by J. R. Buchler (Kluwer Academic, Dordrecht 1990), pp. 269–288.
7. H. Brenner, Dispersion resulting from flow through spatially periodic porous media, *Philos. Trans. R. Soc. London Ser. A* **297**, 81 (1980).
8. P. C. Carman, Fluid flow through granular beds, *Trans. Inst. Chem. Eng.* **15**, 150 (1937).
9. A. J. Chorin, Numerical study of slightly viscous flow, *J. Fluid Mech.* **57**, 785 (1973).
10. J. H. Cushman, *The Physics of Fluids in Hierarchical Porous Media: Angstroms to Miles* (Kluwer Academic, Boston, 1997).
11. R. A. Freeze and J. A. Cherry, *Groundwater* (Prentice Hall, Englewood Cliffs, NJ, 1979).
12. J. J. Fried, *Groundwater Pollution* (American Elsevier, New York, 1975).
13. J. J. Fried and M. A. Combarnous, Dispersion in porous media, *Adv. Hydrosci.* **7**, 169 (1971).
14. L. W. Gelhar, C. Welty, and K. R. Rehfeldt, A critical review of data on field-scale dispersion in aquifers, *Water Resources Res.* **28**(7), 1955 (1992).
15. R. A. Gingold and J. J. Monaghan, Smoothed particle hydrodynamics: Theory and application to non-spherical stars, *Mon. Not. R. Astron. Soc.* **181**, 375 (1977).
16. F. J. M. Horn, Calculation of dispersion coefficients by means of moments, *AIChE J.* **17**, 613 (1971).
17. R. N. Horne and F. Rodriguez, Dispersion of tracer flow in fractured geothermal systems, *Geophys. Res. Lett.* **10**(4), 289 (1983).
18. L. C. Hull, J. D. Miller, and T. M. Clemo, Laboratory and simulation studies of solute transport in fracture networks, *Water Resources Res.* **23**(8), 1505 (1987).
19. D. L. Koch and J. F. Brady, Dispersion in fixed beds, *J. Fluid Mech.* **154**, 399 (1985).
20. D. L. Koch and J. F. Brady, A non-local description of advection–diffusion with application to dispersion in porous media, *J. Fluid Mech.* **180**, 387 (1987).
21. A. Lallemand-Barres and P. Peaudecerf, Recherche des relations entre les valeurs mesurees de la dispersivite macroscopique d'un milieu aquifere, ses autres caracteristiques et les conditions de mesure, *Bull. Bur. Rech. Geol. Min. (BRGM), Ser. 2, Sec. III* **4**, 277 (1978).
22. L. B. Lucy, A numerical approach to the testing of the fission hypothesis, *Astron. J.* **82**(12), 1013 (1977).
23. R. S. Maier, D. M. Kroll, H. T. Davis, and R. S. Bernard, Pore-scale flow and dispersion, *Int. J. Mod. Phys. C* **9**(8), 1523 (1998).
24. G. Matheron and G. De Marsily, Is transport in porous media always diffusive? A counter example, *Water Resources Res.* **16**(5), 901 (1980).
25. J. J. Monaghan, Smoothed particle hydrodynamics, *Annu. Rev. Astron. Astrophys.* **30**, 543 (1992).
26. J. J. Monaghan, *Heat Conduction with Discontinuous Conductivity*, Applied Mathematics Reports and Preprints, 95/18 (Monash University, Australia, 1995).
27. J. P. Morris, P. J. Fox, and Y. Zhu, Modeling low Reynolds number incompressible flows using SPH, *J. Comput. Phys.* **136**, 214 (1997).
28. J. P. Morris, Y. Zhu, and P. J. Fox, Parallel simulations of pore-scale flow through porous media, *Comput. Geotechnics* **25**, 227 (1999).
29. A. Ogata, *Theory of Dispersion in a Granular Medium*, Technical report, U.S. Geological Survey Professional Paper 411-I (1970).

30. T. K. Perkins and O. C. Johnston, A review of diffusion and dispersion in porous media, *Soc. Petrol. Eng. J.* **3**, 70 (1963).
31. J. F. Pickens and G. E. Grisak, Modeling of scale-dependent dispersion in hydrogeologic systems, *Water Resources Res.* **17**(6), 1701 (1981).
32. O. A. Plumb and S. Whitaker, Dispersion in heterogeneous porous media, *Water Resources Res.* **24**(7), 913 (1988).
33. C. D. Shackelford, Limitations to contaminant transport modeling in waste geotechnics, *Geotechnical News* **2**, 50 (1989).
34. L. Smith and F. W. Schwartz, Mass transport. 1. A stochastic analysis of macroscopic dispersion, *Water Resources Res.* **16**(2), 303 (1980).
35. G. Taylor, Dispersion of soluble matter in solvent flowing slowly through a tube, *Philos. Trans. R. Soc. London Ser. A* **219**, 186 (1953).
36. A. F. B. Tompson, On a new functional form for the dispersive flux in porous media, *Water Resources Res.* **24**(11), 1939 (1988).
37. H. F. Wang and M. P. Anderson, *Introduction to Groundwater Modeling: Finite Difference and Finite Element Methods* (Freeman, San Francisco, 1982).
38. Y. Zhu, *A Pore-Scale Study of Flow and Transport through Porous Media*. Ph.D. thesis (Purdue University, 1999).
39. Y. Zhu and P. J. Fox, Smoothed particle hydrodynamics model for diffusion through porous media, *Transport Porous Media* **43**(3), 441 (2001).
40. Y. Zhu, P. J. Fox, and J. P. Morris, A pore-scale numerical model for flow through porous media, *Int. J. Numer. Anal. Methods Geomech.* **23**, 881 (1999).
41. S. Zimmermann, P. Koumoutsakos, and W. Kinzelbach, Simulation of pollutant transport using a particle method, *J. Comput. Phy.* **173**, 322 (2001).